



Analytical and computational methodology for modeling spray quenching of solid alloy cylinders

Nikhin Mascarenhas, Issam Mudawar*

Boiling and Two-phase Flow Laboratory (BTPFL), School of Mechanical Engineering, Purdue University, West Lafayette, IN 47907, USA

ARTICLE INFO

Article history:

Received 28 April 2010

Received in revised form 24 June 2010

Accepted 24 June 2010

Available online 20 August 2010

Keywords:

Quenching

Heat diffusion

Spray cooling

ABSTRACT

Heat-treating of solid alloy cylinders is an important practical problem for which no optimal production methods have been developed, especially in terms of the most crucial quenching stage. This study explores the use of spray quenching as an alternative to the commonly used bath quenching, which is known to yield relatively slow quench rates and provide few options for spatial optimization of cooling rate. A carefully configured spray cooling system is examined, which provides maximum coverage of the surface of a solid alloy cylinder with full-cone pressure sprays. A new analytical model is derived to determine the shape and size of the spray impact zone, as well as the distribution of volumetric flux across the curved surface of the cylinder. This distribution is combined with heat transfer correlations for all spray boiling regimes to generate a local boiling curve for every location across the impact surface. Using these boiling curves as boundary conditions, a transient analysis is conducted for aluminum alloy and steel cylinders. Increasing the nozzle pressure drop or decreasing the orifice-to-surface distance are shown to hasten the exit from the poor film boiling regime to the more efficient transition boiling regime, resulting in a quicker quench. Relatively high thermal diffusivity causes faster transmission of the spray cooling effect through the cylinder and milder temperature gradients in aluminum compared to steel. This also causes the outer surface to cool earlier but deeper points much slower for steel. Large temperature gradients are encountered on the surface during the quench because of different boiling regimes occurring at different locations exposed to the spray. This study highlights several practical advantages of spray quenching compared with bath quenching, including the ability to achieve a wide range of fast quench rates, uniformity and predictability of quench rate, and the ability to predict and guard against imperfections caused by thermal stresses.

© 2010 Elsevier Ltd. All rights reserved.

1. Introduction

Sprays are widely used for rapid cooling of metal surfaces from very high temperatures [1,2]. They are also applied in low temperature applications, which require removal of high heat fluxes from small surfaces [3,4]. The simplest and most widely used sprays in industry are pressure sprays, which achieve droplet breakup by forcing liquid at high pressure through a small orifice—a plain-orifice spray nozzle. The high upstream pressure provides the necessary liquid momentum to overcome surface tension forces, resulting in a cone of finely dispersed droplets characterized by large interfacial area to volume ratio. This important attribute, combined with high droplet impact speed and multiple droplet impact over a relatively large surface area, enables sprays to achieve high rates of heat removal while maintaining fairly uniform surface temperatures.

One of the most important industrial applications of spray cooling is quenching of aluminum alloy and steel parts. Quenching is

the most critical stage of heat-treating, which is intended to alter the alloy's microstructure in pursuit of superior mechanical properties. Heat-treating is comprised of three stages: solution heat-treating, quenching and age-hardening [5,6]. Solution heat-treating involves heating the alloy close to the liquidus temperature to enable the alloying elements to diffuse into the grains of the primary metal. This is followed by rapid quenching to retain the alloying elements in a supersaturated solid solution. Age hardening is accomplished by reheating the alloy below solvus temperature for a specified period, resulting in a fine dispersion of precipitates within the grains of the primary metal. These fine precipitates produce an alloy with maximum hardness and maximum strength.

Implementation of quenching is by far the most critical and challenging stage of heat-treating. A slow quench rate could result in massive precipitation along the primary metal grain boundaries rather than within the grains, producing a microstructure that cannot be improved upon by age-hardening. Conversely, a very fast quench rate might induce large variations in cooling rate between thin versus thick sections of a complex-shaped part, resulting in severe residual stresses. Both slow and non-uniform quenching are commonly encountered with bath quenching, where no means

* Corresponding author. Tel.: +1 765 494 5705; fax: +1 765 494 0539.
E-mail address: mudawar@ecn.purdue.edu (I. Mudawar).

Nomenclature

a	half-length of major diameter of elliptical impact area	T_f	spray liquid temperature
A	area formed by projecting spherical surface A' on surface of cylinder	T_s	surface temperature
A'	area of spherical surface bound by spray's cone angle and centered at spray orifice, and whose radius is equal to distance from orifice-to-surface of cylinder	T_{sat}	saturation temperature
b	half-length of minor diameter of elliptical impact area	ΔT	difference between surface and liquid temperatures, $T_s - T_f$
CHF	critical heat flux	ΔT_{sub}	subcooling of spray liquid, $T_{sat} - T_f$
c_p	specific heat at constant pressure	U_m	mean droplet velocity
D	diameter of solid alloy cylinder	We_{d_o}	Weber number based on nozzle's orifice diameter
d_o	diameter of nozzle's orifice	x	coordinate defined in Fig. 3
d_{32}	Sauter mean diameter	z	coordinate defined in Fig. 3
h	heat transfer coefficient	<i>Greek symbols</i>	
H	distance from orifice-to-surface of cylinder	β	angle defined in Fig. 4
h_{fg}	latent heat of vaporization	γ	angle defined in Fig. 4
k	thermal conductivity	θ	cone angle of spray
K	nozzle's flow coefficient	μ	viscosity
$Nu_{d_{32}}$	Nusselt number based on d_{32} , hd_{32}/k_f	ρ	density
ΔP	pressure drop across spray nozzle	σ	surface tension
Pr	Prandtl number	φ	half-angle of unit cell as defined in Fig. 4
Q	total volumetric flow rate of spray	<i>Subscripts</i>	
Q''	local volumetric flux across surface	a	ambient air
Q''_{sp}	uniform volumetric flux along spherical surface bound by spray's cone angle and centered at spray nozzle's orifice, and whose radius is equal to distance from orifice-to-surface of cylinder	CHF	critical heat flux
q''	heat flux	DFB	departure from film boiling
$q''_{m,p}$	local (point-based) critical heat flux	f	liquid
r	coordinate defined in Fig. 3	g	vapor
Re_{d_o}	Reynolds number based on nozzle's orifice diameter	MIN	minimum heat flux (Leidenfrost point)
$Re_{d_{32}}$	Reynolds number based on d_{32} , $\rho_f Q'' d_{32} / \mu_f$	OSP	onset of single-phase liquid cooling
T	temperature	s	cylinder's surface
		sat	saturation
		sub	subcooling

are available to control local cooling rate for different regions of the alloy surface. This is where spray cooling can play a very beneficial role in the heat-treating industry, by providing localized control over cooling rate through changes in any number of spray parameters, such as supply pressure or orifice-to-surface distance. Using an arrangement of optimally configured sprays, a complex-shaped alloy part may be cooled uniformly by impacting thick sections of the part with dense sprays and thin sections with light [5,6].

However, accurate prediction of the quench curve (also called temperature–time cooling curve) at every point in a three-dimensional metal alloy part that is subjected to spray cooling is a very illusive task, complicated by:

- (1) Temporal changes in cooling regime occurring on the sprayed surface during the quench, which are represented by the various boiling regimes corresponding to the spray's boiling curve.
- (2) Spatial variations in cooling rate within each boiling regime resulting from non-uniform distributions of key spray parameters (e.g., droplet diameter, volumetric flux) upon impact with the part's surface.
- (3) Contribution of three-dimensional heat diffusion within the part itself.

To simplify the discussion of these contributions, the effects of the temporal changes and three-dimensional heat diffusion effects are discussed first for the simple case of bath quenching to determine the relationship between the boiling curve and the quench curve. The effects of spatial variations associated with spray parameters are discussed afterwards.

1.1. Boiling curve and quench curve

Cooling rate of an object during bath quenching is non-uniform and can be demarcated into distinct regimes on the basis of the phenomena driving the cooling. These regimes are illustrated in the boiling curve shown in Fig. 1(a). For metal heat-treating operations, quenching is initiated at an elevated temperature corresponding to the film boiling regime, well in excess of the saturation temperature for water. In this regime, a thin vapor layer quickly encases the surface of the part, precluding any direct contact with liquid. Heat from the surface is both conducted and radiated across the vapor layer before evaporating the liquid. The large thermal resistance of the vapor layer is responsible for very poor heat transfer coefficients within the film boiling regime. It should be noted that, in the case of spray quenching, the thin vapor layer could form beneath individual droplets upon impact with the surface. The minimum heat flux point (commonly referred to as the Leidenfrost point) is very important for quenching since it marks the temperature at which the insulating vapor layer begins to break up, allowing partial wetting with liquid and, hence, improved cooling rate, within the transition boiling regime. The entire surface becomes available to liquid wetting after the critical heat flux (CHF) point. In the ensuing nucleate boiling regime, very high heat removal rates are achieved due to both vigorous boiling and full liquid contact. Eventually, cooling rate decreases appreciably as the boiling completely subsides with the surface entering the final single-phase cooling regime.

One way to introduce the quench curve is to consider a small metal part that satisfies the criterion of very small Biot number (i.e., maintains isothermal behavior) during every boiling regime.

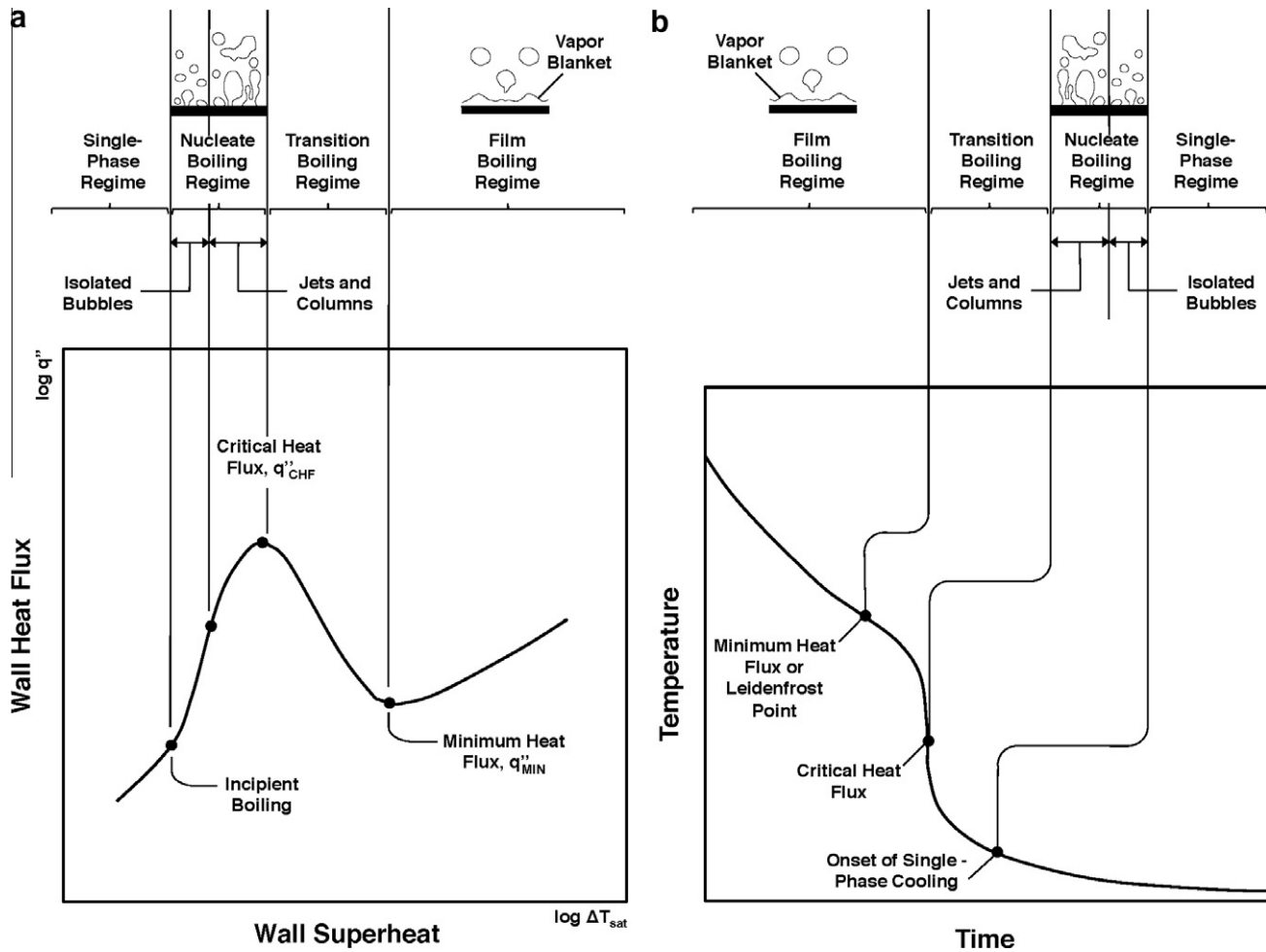


Fig. 1. (a) Boiling curve and (b) corresponding quench curve.

Equating the rate of thermal storage to the heat removal rate as the part encounters the succession of boiling regimes depicted in Fig. 1(a) yields a quench curve of the shape shown in Fig. 1(b). The quench curve clearly captures the cooling rates associated with the individual regimes: slow for film boiling, faster for transition boiling following the Leidenfrost point, fastest for nucleate boiling, and slow again for single-phase cooling. However, there is a fundamental difference between the boiling curve and quench curve. For a given coolant and metal, the boiling curve is a surface phenomenon and, therefore, independent of thermal mass of the part. On the other hand, the quench curve is highly dependent on thermal mass and, unlike the example just discussed, will vary spatially within large objects.

1.2. Spray parameters and their spatial distributions

The first step to understanding spray quenching is to examine the key spray parameters that have been identified in prior studies as influencing cooling performance in one or more of the spray boiling regimes. The three parameters reported as having the most significant influence are volumetric flux, Q' , Sauter mean diameter, d_{32} , and mean droplet velocity, U_m [1,2,5–8]. Perhaps the most important of all spray parameters, volumetric flux is the amount of spray liquid impinging upon the surface per unit area per unit time, and has the units of velocity. Sauter mean diameter (SMD) is defined as the diameter of a drop having the same volume to surface area ratio as the spray, and is measured with the aid of any number of optical spray diagnostic instruments.

One of the most challenging tasks in predicting the quench curve for metallic parts that are subjected to spray cooling is accurate accounting for the spatial distributions of the spray parameters. For plain-orifice pressure sprays, a finite albeit short distance is required downstream of the orifice for the droplet breakup process to develop and the orifice-to-surface distance is always maintained greater than this distance to achieve reliable and predictable cooling behavior. Downstream from the droplet breakup region, both d_{32} and U_m are fairly constant both along the spray axis and away from the axis for orifice-to-surface distances of practical interest. However, Q' decreases appreciably along the spray axis away from the orifice; it also decreases away from the axis. Because of the strong dependence of cooling rate on Q' in several boiling regimes, these spatial variations must be taken into consideration when configuring a spray quenching system. These spatial variations have been modeled analytically for a spray impacting a flat surface [9]. This model was combined with correlations based on the spray parameters to accurately predict spray cooling behavior corresponding to nucleate boiling and CHF [10,11].

1.3. Quenching of alloy cylinders

In the course of aluminum alloy and steel production, the solidified alloy blanks are either forged or extruded, commonly into rounds (cylindrical rods) requiring heat treatment. Studies addressing the influence of spray quenching on rods are quite sparse. Hodgson et al. [12] experimentally studied cross-flow of

water–air spray across a brass cylinder at different flow rates. Droplet evaporation was purposely suppressed prior to surface impact by eliminating the water–air temperature difference, preserving the two-component nature of the spray. They found that the side of the cylinder’s surface directly impacted by the spray achieved better cooling, and the cooling rate increased with liquid-to-air mass flow ratio. Albright [13] devised a controlled environment wind tunnel that exposed the curved surface of a 5.08 cm diameter solid steel cylinder at 95 °C to a water–air spray. They concluded that spray cooling is substantially more efficient than bath cooling. Heat transfer increased drastically by increasing the spray flow rate as well as with optimal orientation of the cylinder surface relative to the spray. Buckingham and Haji-Sheikh [14] experimentally investigated the quenching of a 316 stainless steel cylinder from 1000 °C by a single water–air spray that encompassed the entire cylinder. Like Hodgson et al. and Albright, they showed that the projected surface area normal to the spray axis and directly impacted by the spray achieved superior cooling, and overall cooling effectiveness increased with increasing mass flow rate of water.

Other investigators have also examined water–air spray cooling of rods and tube bundles (heat exchangers) at different orientations using a variety of coolants such as R-141b, R-134a, R-123 and water [14–20]. These studies were prompted by the need for analysis of evaporation and de-humidification effects across cylindrical evaporators in refrigeration systems.

1.4. Objectives of study

Overall, the findings of Hodgson et al., Albright, and Buckingham and Haji-Sheikh emphasize the need for (1) determining the spatial variations of spray liquid impact on cylindrical surfaces, (2) predicting the influence of the spatial variations of spray cooling rate, and more importantly, (3) developing a strategy for implementing spray cooling in the quenching of metal alloy rods in an optimal and predictable manner as a substitute for conventional bath quenching. These are precisely the objectives of the present study.

2. Spray cooling system and unit cell

Shown in Fig. 2, the system considered in this study consists of a solid metal alloy cylinder that is subjected to an array of identical plain-orifice pressure sprays. Maximum surface exposure to the liquid is achieved by arranging the sprays circumferentially as well as longitudinally such that their impact areas on the cylindrical surface are tangent to one another and do not overlap. Another

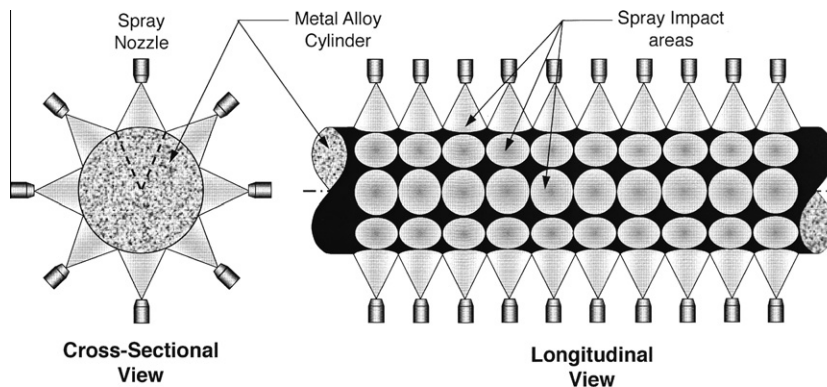


Fig. 2. Spray nozzle configuration for quenching of solid metal alloy cylinder.

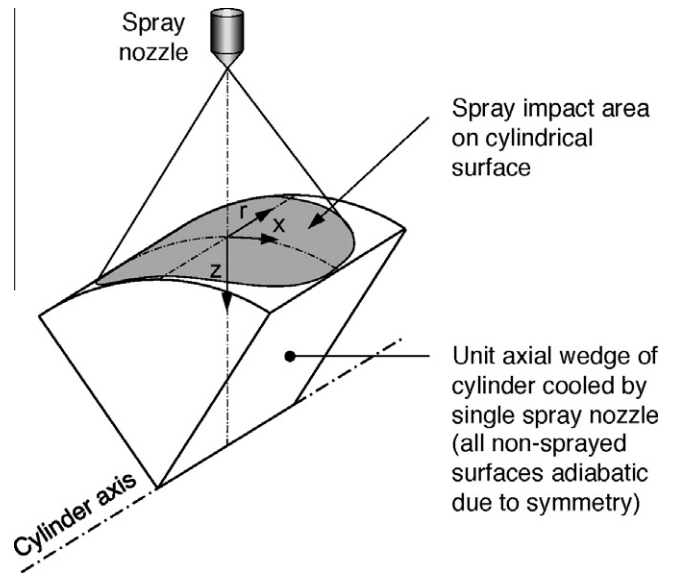


Fig. 3. Unit cell modeled in present study.

advantage of this configuration is the ease of determining spray nozzle layout in a heat-treating plant.

Fig. 3 shows a representative unit cell of the system, consisting of an extruded sector of the cylinder subjected to a single spray. Cooling is achieved within the spray impact area, outside of which the cooling is assumed comparatively negligible. All other surfaces of the unit cell can be assumed perfectly insulated due to symmetry.

In the present study, a cylinder of diameter $D = 0.5$ m and full-cone plain-orifice spray nozzles with a cone angle of $\theta = 45^\circ$ are examined, and the nozzle pressure, ΔP , and the orifice-to-surface distance, H , are both varied. Materials considered in the analysis are aluminum 2024 and steel (ASTM A322). The spray fluid is water, which is supplied at $T_f = 23$ °C, and the cylinder cell is assumed initially at a uniform temperature of 427 °C. The characteristics of the water spray nozzles (at 23 °C) and properties of two alloys are given in Tables 1 and 2, respectively.

3. Volumetric flux distribution model for cylindrical surface

As indicated earlier, volumetric flux is the spray parameter most commonly cited as influencing spray cooling rate. This is also the spray parameter that exhibits the strongest spatial variation. Hence, accurate prediction of quench behavior for alloy cylinders

The spray volumetric flux along the curved impact surface can be obtained by combining Eqs. (1), (2) and (8).

$$Q'' = Q''_{sp} \frac{dA'}{dA} = \frac{Q}{2\pi H^2 [1 - \cos(\theta/2)]} \cos^3 \gamma \left[\frac{D}{4H} \{ \sin \beta \cot \gamma - \cos \beta \cos^2 \gamma + \cos^2 \gamma \left(\frac{2H}{D} + 1 \right) \frac{1}{1 - \tan \beta \tan \gamma} \} \right]^{-1} \quad (9)$$

Fig. 4 shows that the half-angle of the cylinder's unit cell is related to the spray's cone angle by the relation (obtained using sine rule)

$$\varphi = \sin^{-1} \left\{ \left(\frac{2H}{D} + 1 \right) \sin(\theta/2) \right\} - \theta/2, \quad (10)$$

and outer edge of the spray's impact area is an ellipse whose major and minor diameters are given, respectively, by

$$2a = D \sin \varphi \quad (11)$$

and

$$2b = 2H \tan(\theta/2). \quad (12)$$

The mean volumetric flux across an *equivalent flat impact area* (not true curved impact area) is given by and

$$\bar{Q}'' = \frac{Q}{\pi ab} = \frac{Q}{\pi \{ H \tan(\theta/2) \} \left\{ \frac{D}{2} \sin \varphi \right\}} \quad (13)$$

Applying the above expression $r = H \tan \gamma$ (from Fig. 4) simplifies Eq. (9) to

$$\frac{Q''}{\bar{Q}''} = \left[\frac{\tan(\theta/2) \sin \varphi}{1 - \cos(\theta/2)} \right] \frac{1}{\left\{ 1 + \left(\frac{r}{H} \right)^2 \right\}^{3/2}} \times \left\{ \frac{\sin \beta}{\left(\frac{r}{H} \right)} - \frac{\cos \beta}{1 + \left(\frac{r}{H} \right)^2} + \frac{1}{1 + \left(\frac{r}{H} \right)^2} \left(\frac{2H}{D} + 1 \right) \frac{1}{1 - \left(\frac{r}{H} \right) \tan \beta} \right\}^{-1}, \quad (14)$$

where

$$\beta = \sin^{-1} \left\{ \left(\frac{2H}{D} + 1 \right) \frac{\left(\frac{r}{H} \right)}{\sqrt{1 + \left(\frac{r}{H} \right)^2}} \right\} - \tan^{-1} \left(\frac{r}{H} \right). \quad (15)$$

Fig. 5(a)–(c) show the volumetric distribution along the curved impact surface of the cylinder for different values of nozzle pressure drop, ΔP . A common trend among all three conditions is a rather flat Q'' profile near the spray axis, with a maximum at $r = 0$, decreasing by only 7–8% at $r = 0.4b$ compared to 40–50% at $r = b$. The peak value of Q'' at $r = 0$ increases with increasing ΔP because the total spray flow rate, Q , also increases with increasing ΔP . Figs. 5(a) and 6(a)–(b) show the peak value at $r = 0$ also increases with decreasing orifice-to-surface distance, H . This trend is readily apparent from Eq. (2), which shows that smaller distances concentrate more of the spray over a given impact area. The same figures show the impact area decreasing with decreasing H . However, the total spray rate, Q , reaching the surface is unchanged because ΔP is the same for all three cases. The nozzle height values (268 mm, 305 mm and 354 mm) selected in these plots ensure that the entire circumference of the cylinder is impacted by a fixed number of sprays, 6, 5 and 4, respectively.

4. Spray boiling curves

Correlations describing the relationship between local heat flux and surface temperature during spray cooling have been developed for all boiling regimes at the Purdue University Boiling and two-phase flow laboratory since the late 1980s [5–7,9–11,21,23,24] and are summarized in Table 3. The spray heat transfer correlations are dependent on the spray's local volumetric flux, Q'' , mean droplet diameter, d_{32} , mean droplet velocity, U_m , and liquid properties. Aside from the boiling regimes and transition points indicated in Fig. 1(a) and (b), Table 3 includes a 'film wetting' regime, a region incurring slight collapse of the vapor layer that occurs towards the lower temperature range of film boiling regime and extends to the minimum heat flux point. This regime is accounted for in the form of a cubic expression that ensures a continuous and differentiable boiling curve at this regime's transition points [24].

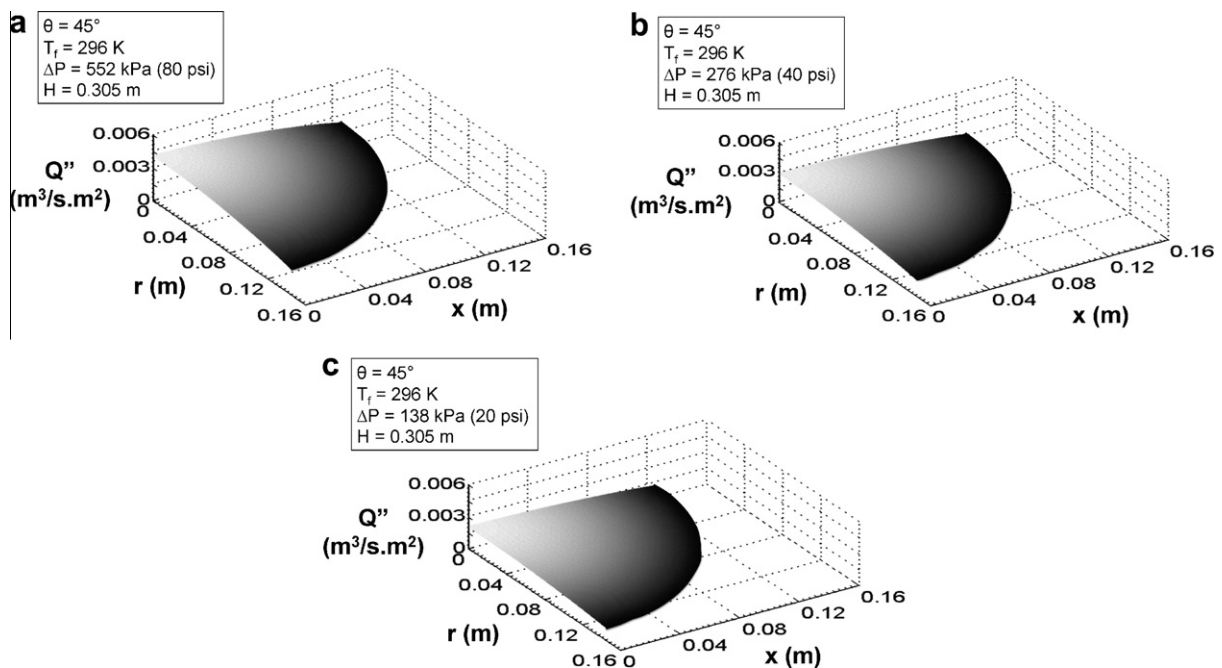


Fig. 5. Volumetric flux distributions for $H = 0.305$ m with (a) $\Delta P = 552$ kPa (80 psi), (b) $\Delta P = 276$ kPa (40 psi), and (c) $\Delta P = 138$ kPa (20 psi).

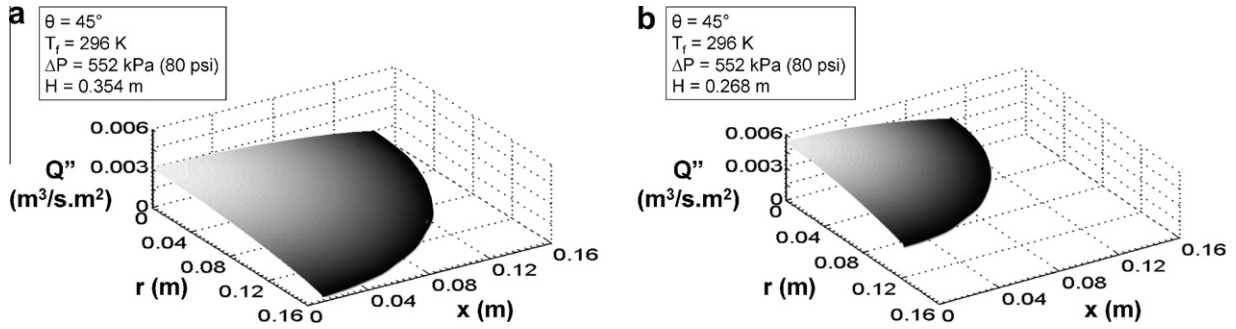


Fig. 6. Volumetric flux distributions for $\Delta P = 552$ kPa (80 psi) with (a) $H = 0.354$ m and (b) $H = 0.268$ m.

Table 3
Spray quenching heat transfer correlations.

Boiling regime or Transition point	Correlation
Single phase [7,10]:	$T_{OSP} = 13.43Re_{d32}^{0.167}Pr_f^{0.123}\left(\frac{k_f}{d_{32}}\right)^{0.22} + T_f$ $Nu_{d32} = 4.7Re_{d32}^{0.61}Pr_f^{0.32}$
Nucleate boiling [10]:	$\frac{q''_{d32}}{\mu_f h_{fg}} = 0.00479\left\{\frac{c_{pf}(T_s - T_f)}{h_{fg}}\right\}^{5.75}\left(\frac{\rho_f}{\rho_g}\right)^{2.5}\left(\frac{\mu_f \bar{Q}'' d_{32}}{\sigma}\right)^{0.35}$
Critical heat flux [10]:	$\frac{q''_{CHF}}{\rho_g h_{fg} Q''} = 2.3\left(\frac{\rho_L}{\rho_g}\right)^{0.3}\left(\frac{\rho_f Q'' d_{32}}{\sigma}\right)^{-0.35}\left(1 + 0.0019\frac{\rho_f c_{pf} \Delta T_{sub}}{\rho_g h_{fg}}\right)$
Transition boiling [23]:	$q'' = q''_{CHF} - \frac{q''_{CHF} - q''_{MIN}}{(\Delta T_{CHF} - \Delta T_{MIN})^3} \left[3\Delta T_{CHF}^3 - 3\Delta T_{CHF}^2 \Delta T_{MIN} + 6\Delta T_{CHF} \Delta T_{MIN} \Delta T - 3(\Delta T_{CHF} + \Delta T_{MIN}) \Delta T^2 + 2\Delta T^3 \right]$
Minimum heat flux [23]:	$q''_{MIN} = 3.324 \times 10^6 Q''^{0.544} U_m^{0.324}$ $\Delta T_{MIN} = 2.049 \times 10^2 Q''^{0.066} U_m^{0.138} d_{32}^{-0.035}$
Film wetting [24]:	$q'' = q''_{MIN} + \frac{q''_{DFB} - q''_{MIN}}{(\Delta T_{DFB} - \Delta T_{MIN})^3} \left[(3\Delta T_{DFB} - \Delta T_{MIN}) \Delta T_{MIN}^2 - 6\Delta T_{DFB} \Delta T_{MIN} \Delta T + 3(\Delta T_{DFB} + \Delta T_{MIN}) \Delta T^2 - 2\Delta T^3 \right] + \frac{\partial q''}{\partial \Delta T} \Big _{DFB} \frac{1}{(\Delta T_{DFB} - \Delta T_{MIN})^2} \left[-\Delta T_{DFB} \Delta T_{MIN}^2 + (2\Delta T_{DFB} + \Delta T_{MIN}) \Delta T_{MIN} \Delta T - (\Delta T_{DFB} + 2\Delta T_{MIN}) \Delta T^2 + \Delta T^3 \right]$ $\frac{\partial q''}{\partial \Delta T} \Big _{DFB} = 1.164 \times 10^4 Q''^{0.397} U_m^{0.0995} d_{32}^{-0.0366}$ $q''_{DFB} = 6.1 \times 10^6 Q''^{0.589} U_m^{0.244}$ $\Delta T_{DFB} = 886.2 Q''^{0.192} U_m^{0.144} d_{32}^{0.0367}$
Film boiling [23]	$q'' = 63.25 \Delta T^{1.691} Q''^{0.264} d_{32}^{-0.062}$

Units: q'' [$W m^{-2}$], $\Delta T = T_s - T_f$ [$^{\circ}C$], Q'' [$m^3 s^{-1} m^{-2}$], U_m [$m s^{-1}$], d_{32} [m], h [$W m^{-2} K^{-1}$], ρ_f [$kg m^{-3}$], h_{fg} [$J kg^{-1}$], c_{pf} [$J kg^{-1} K^{-1}$], k_f [$W m^{-1} K^{-1}$], μ_f [$N s m^{-2}$], σ [$N m^{-1}$] ($T_s + T_f$)/2 is used in single-phase regime and saturation temperature in other regimes to evaluate fluid properties.

Notice that when applying the CHF relation given in Table 3, CHF is assumed to occur first along the outer rim of the spray impact area along the major axis, where Q'' is lowest.

The mean droplet diameter is determined from the nozzle pressure drop, ΔP , and orifice diameter, d_o , based on the following correlation for full-cone spray nozzles [11],

$$\frac{d_{32}}{d_o} = 3.67 \left[We_{d_o}^{1/2} Re_{d_o} \right]^{-0.259} \quad (16)$$

In Eq. (16), the Weber and Reynolds numbers are defined as

$$We_{d_o} = \frac{\rho_a (2\Delta P / \rho_f) d_o}{\sigma} \quad (17)$$

and

$$Re_{d_o} = \frac{\rho_f (2\Delta P / \rho_f)^{1/2} d_o}{\mu_f} \quad (18)$$

The nozzle data from Table 1 were used in Eqs. (14) and (16) to determine Q'' and d_{32} , respectively, which when inserted into the correlations given in Table 3, yield local transient relations

between the spray cooling heat flux and wall temperature for each of the boiling regimes. The mean velocity data required by the correlations are also given in Table 1. The transient relations are used to develop boiling curves for different spray conditions.

Fig. 7 indicates different reference points ($P1-P4$) along the curved surface exposed to the spray away from the spray axis, which are used to illustrate the spatial distribution of the spray's boiling curves, as well as other points both within the same plane ($P5-P7$) and along the axis but internal to the cylinder ($P8-P12$) that are used later to examine the effects of heat diffusion on delayed thermal response to the spray in the form of quench curves for these points.

Fig. 8(a)–(c) show the boiling curves for different values of nozzle pressure drop, ΔP , orifice-to-surface distance, H , and distances from the spray axis across the spray impact surface, respectively. Increasing ΔP or decreasing H is shown shifting all boiling regimes as well as transition points between the different regimes (excepting temperature T_{CHF} corresponding to the CHF point) at the center of the spray to higher surface temperatures, indicating faster overall cooling rates. The opposite trend is evident in Fig. 8(c) for points farther away from the spray axis. These trends can be explained mostly by the increased Q'' achieved by increasing ΔP , decreasing H , or decreasing distance from the spray axis as shown earlier in Figs. 5(a)–(c) and 6(a)–(b). As indicated in Table 3, increasing Q'' increases both q''_{MIN} and ΔT_{MIN} , hastening the onset of transition boiling.

It should be emphasized that, as indicated in the previous section, decreasing H for a fixed ΔP , amounts to using more spray nozzles circumferentially, which, in turn, increases the total flow rate of spray liquid per surface area of the cylinder.

5. Quench curve results and discussion

Because of symmetry, half the unit cell shown in Fig. 3 is considered for transient analysis using ANSYS, which is employed in this study because of its prevalence in the heat-treating industry. This ANSYS analysis is comprised of three stages: pre-processing, solution and post-processing. In the pre-processing stage, all inputs required for analysis are supplied to the system. This includes the model dimensions, material properties and boundary conditions. The boundary conditions in this case are the spray correlations provided in Table 3, as well as insulation outside of the spray impact area and on all four inner surfaces. The solution stage is executed internally by ANSYS as per the criteria set by the user, such as convergence requirements and solution methodology. However, the transient nature of the analysis requires a macro written in ANSYS Parametric Design Language (APDL). This macro repeatedly uses the nodal temperature output at every sub-step as an input to update and apply the spray heat flux on the sprayed surface. The post-processing stage is the output stage, where the

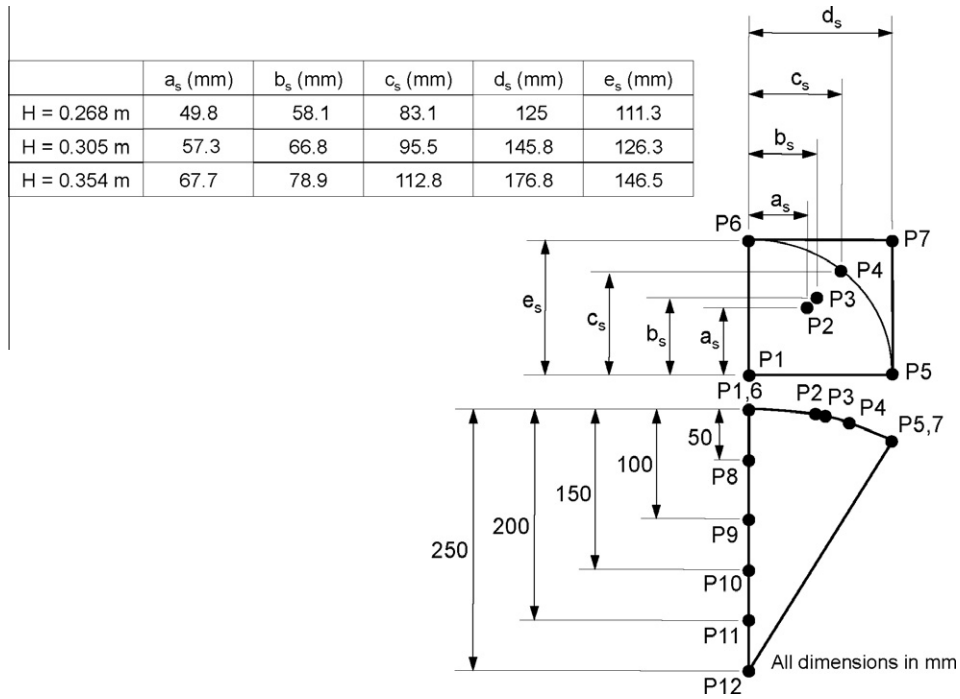


Fig. 7. Locations across outer surface and along central axis of unit cell examined in computational model.

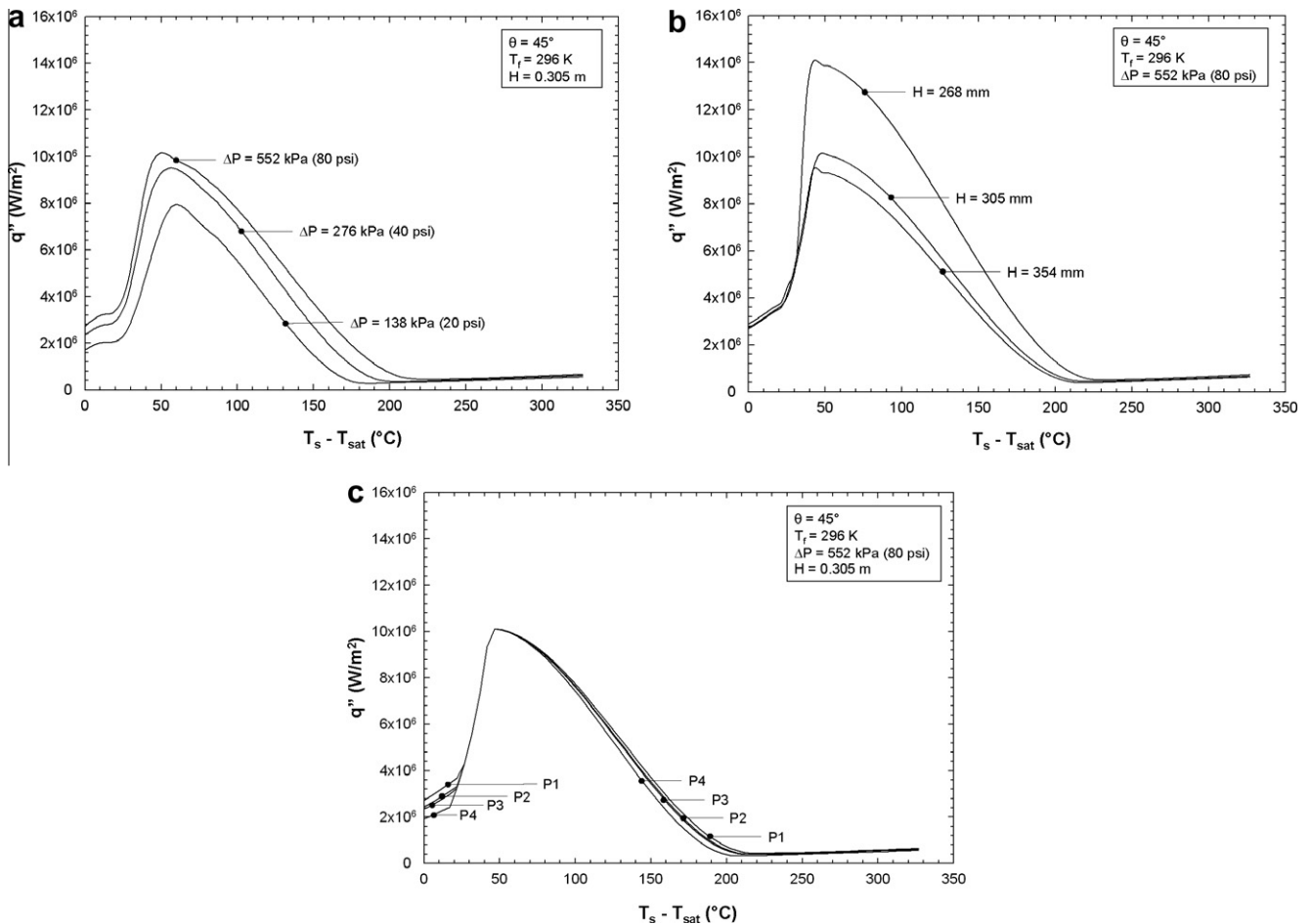


Fig. 8. Variations of spray boiling curve with (a) ΔP for $H = 0.305$ m along spray axis, (b) H for $\Delta P = 552$ kPa (80 psi) along spray axis, and (c) surface location away from spray axis for $\Delta P = 552$ kPa (80 psi) and $H = 0.305$ m.

user may view plots or read lines of output results. Although steel quenching is typically achieved at much higher initial temperatures, the same isothermal initial condition of 427 °C is applied to the entire unit cell for both aluminum alloy and steel based on typical operating conditions for aluminum alloys, and to facilitate direct assessment of material property effects on the quench curve by comparing results for the two alloys. The analysis is terminated when the surface reaches nearly room temperature (25 °C) and the cooling effects are felt at the axis of the cylinder.

Figs. 5(a)–(c) and 6(a)–(b) were used to identify critical locations on the cylinder’s surface having discernable variations in volumetric flux. Fig. 7 shows these and other locations along the axis but within the cylinder that were chosen to develop a general understanding of cooling trends for the entire unit cell.

Figs. 9(a)–(c) and 10(a)–(b) show quench curves for the aluminum alloy cylinder corresponding to all the points indicated in Fig. 7 and different values of nozzle pressure drop, ΔP , and orifice-to-surface distance, H , respectively. Similarly, Figs. 11(a)–(c) and 12(a)–(b) show quench curves for steel for different values of ΔP and H , respectively. Notice in all these plots that points P1–P6 are directly exposed to the spray, while the quench curves for P7–P12 are delayed by heat diffusion effects. This results in different slopes between the two clusters of points, with the first cluster having conventional spray quench curves and the second cluster undergoing more gradual and slower cooling.

Overall, comparing quench curves from Figs. 9(a)–(c) and 10(a)–(b) for aluminum, to those from Figs. 11(a)–(c) and 12(a)–(b) for steel for identical ΔP and H values shows that the locations

exposed to the spray (P1–P6) cool much faster for steel than for aluminum. Conversely, steel exhibits extremely slow cooling rates at the inner locations (P7–P12) compared to aluminum. These trends can be explained by comparing the thermal diffusivities of the two alloys, $8.07 \times 10^{-5} \text{ m}^2/\text{s}$ for aluminum compared to $1.25 \times 10^{-5} \text{ m}^2/\text{s}$ for steel. With its significantly higher diffusivity, the aluminum surface transmits the cooling effect more rapidly from the surface through the unit cell, which reduces cooling rate at the surface and increases it inside the cell compared to steel. On the other hand, relatively poor diffusivity concentrates the cooling effect near the surface for steel, resulting in faster surface cooling rates at the surface, and delays the response within the cell.

These effects can be better understood by contrasting thermal gradients in the z-direction for the two alloys. Fig. 13 clearly shows how, 20 s into the quench, the maximum surface gradient for steel is over 12 times greater than for aluminum. Also shown is that the gradient in steel drops to about 4.4% of the maximum surface value within a much shorter distance from the surface compared to the same percentage drop for aluminum.

Figs. 9(a)–(c), and 9(a), 10(a)–(b) highlight the effects of ΔP and H , respectively, on the quench curve for aluminum. Similar trends are reflected in Figs. 11(a)–(c), and 11(a), 12(a)–(b) for the effects of ΔP and H , respectively, for steel. These curves confirm the trends discussed earlier in conjunction with the boiling curves for the two alloys, that increasing ΔP or decreasing H hasten the onset of transition boiling and rapid cooling rates. Another interesting observation is that, for all surface locations that are directly impacted by the spray, the transition from film boiling to the

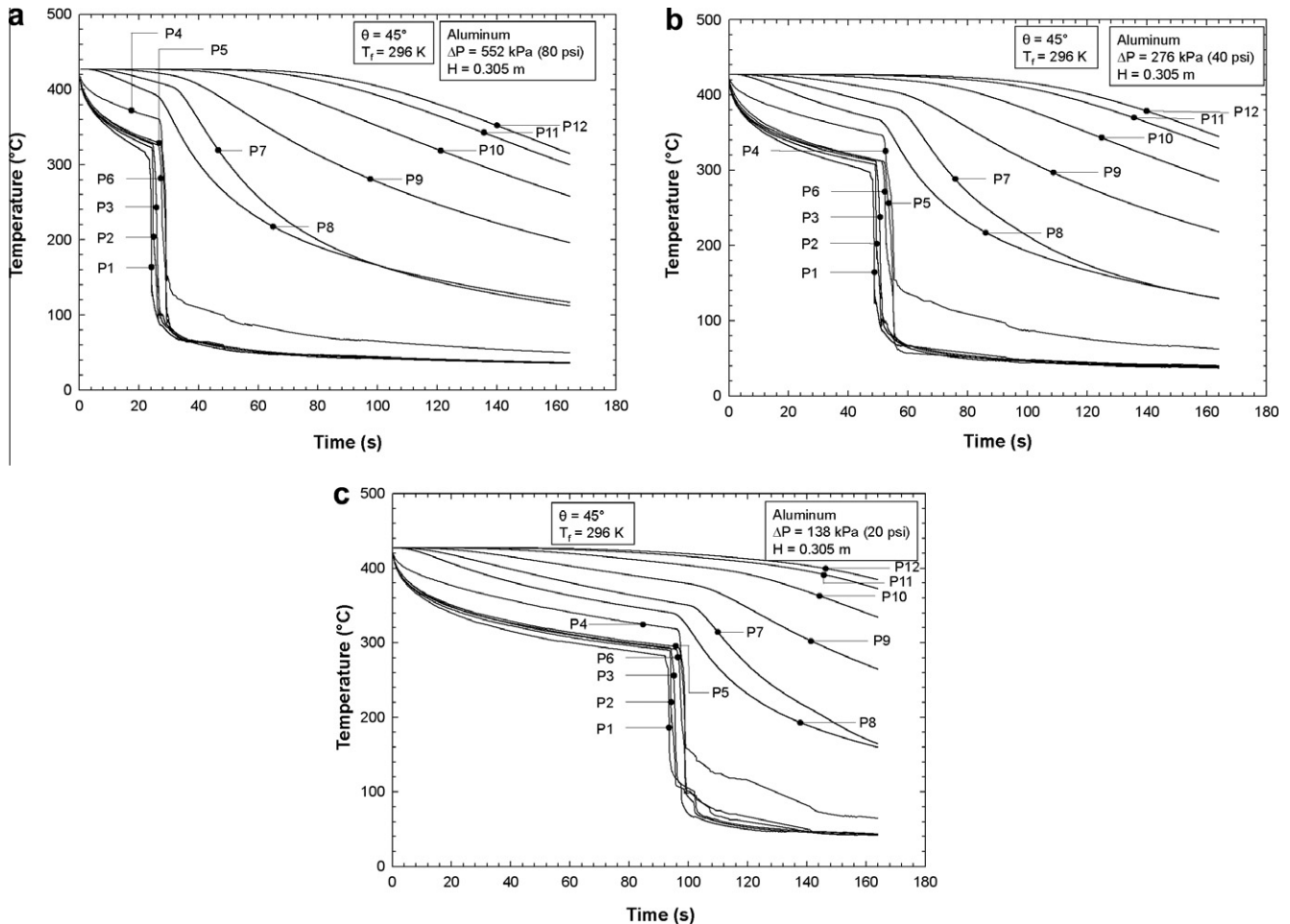


Fig. 9. Spray quench curves for aluminum with $H = 0.305 \text{ m}$ and (a) $\Delta P = 552 \text{ kPa}$ (80 psi), (b) $\Delta P = 276 \text{ kPa}$ (40 psi) and (c) $\Delta P = 138 \text{ kPa}$ (20 psi).

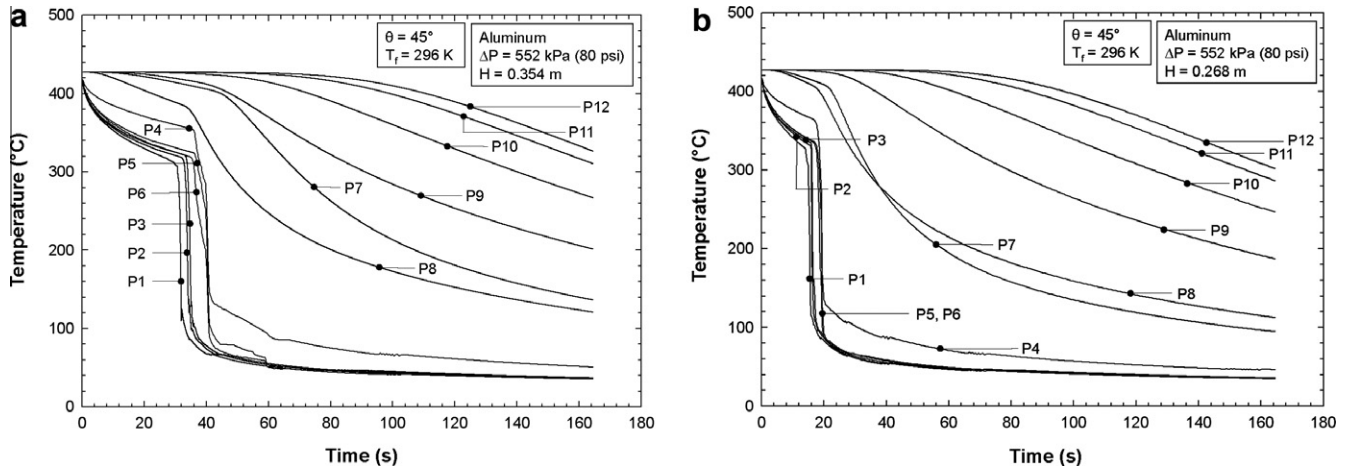


Fig. 10. Spray quench curves for aluminum with $\Delta P = 552$ kPa (80 psi) and (a) $H = 0.354$ m and (b) $H = 0.268$ m.

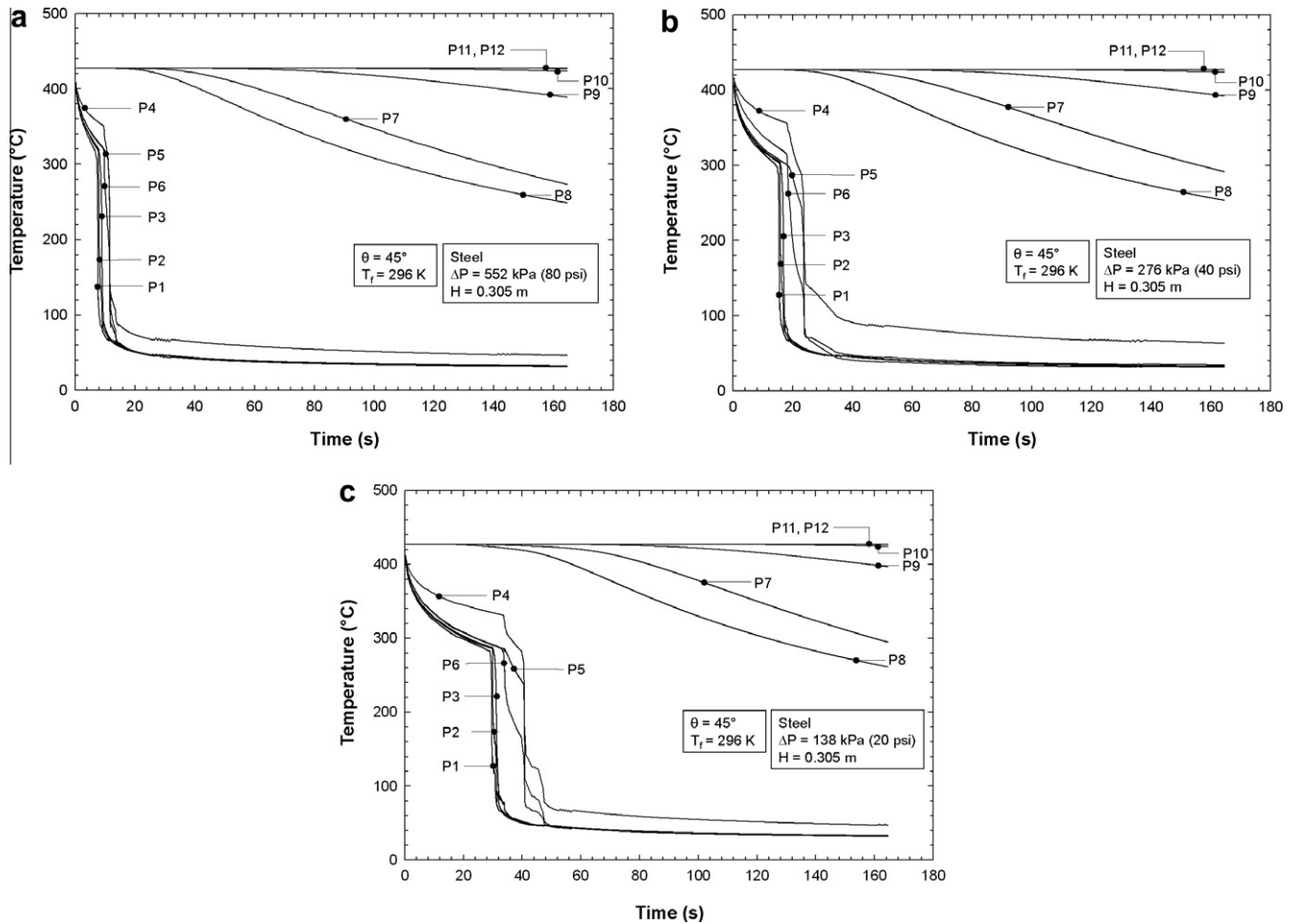


Fig. 11. Spray quench curves for steel with $H = 0.305$ m and (a) $\Delta P = 552$ kPa (80 psi), (b) $\Delta P = 276$ kPa (40 psi) and (c) $\Delta P = 138$ kPa (20 psi).

single-phase regime takes place within about the same duration (~ 7 s for aluminum and ~ 4 s for steel) regardless of the operating conditions examined.

Fig. 14(a)–(f) show surface and near-surface temperature contour plots for aluminum for a specific set of nozzle conditions to illustrate the significance of boiling regime transitions. These plots show that, at any given time, different surface locations can under-

go different boiling regimes, which can produce large surface temperature gradients during the quench. Two spatial features common to all the contour plots are a temperature minimum at the spray axis, and nearly elliptic bands of transition to higher temperatures towards the periphery of the spray impact area.

These results highlight several advantages associated with the application of sprays for quenching of solid cylinders as compared

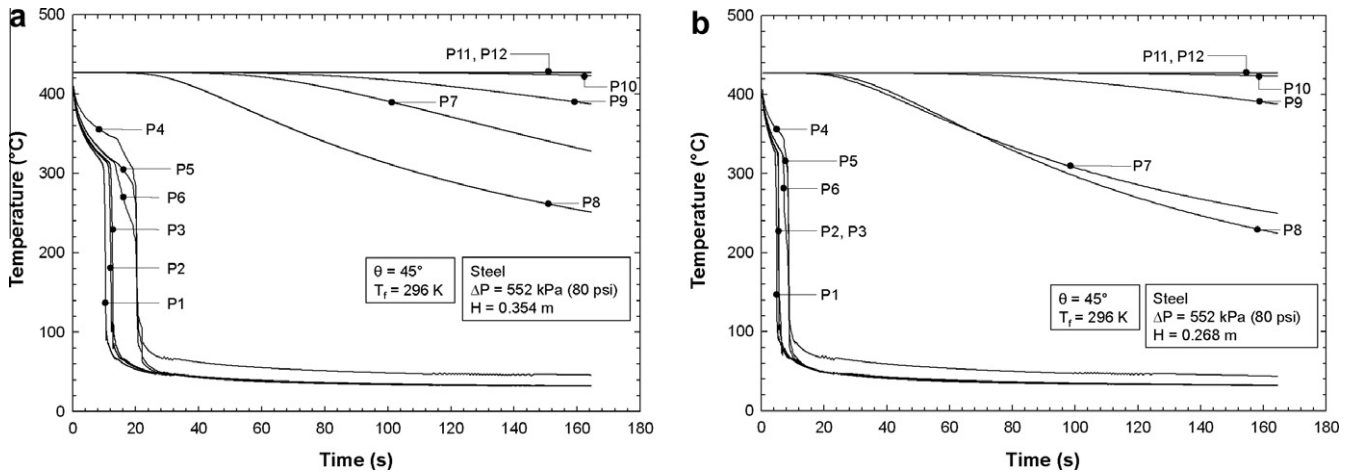


Fig. 12. Spray quench curves for steel with $\Delta P = 552$ kPa (80 psi) and (a) $H = 0.354$ m and (b) $H = 0.268$ m.

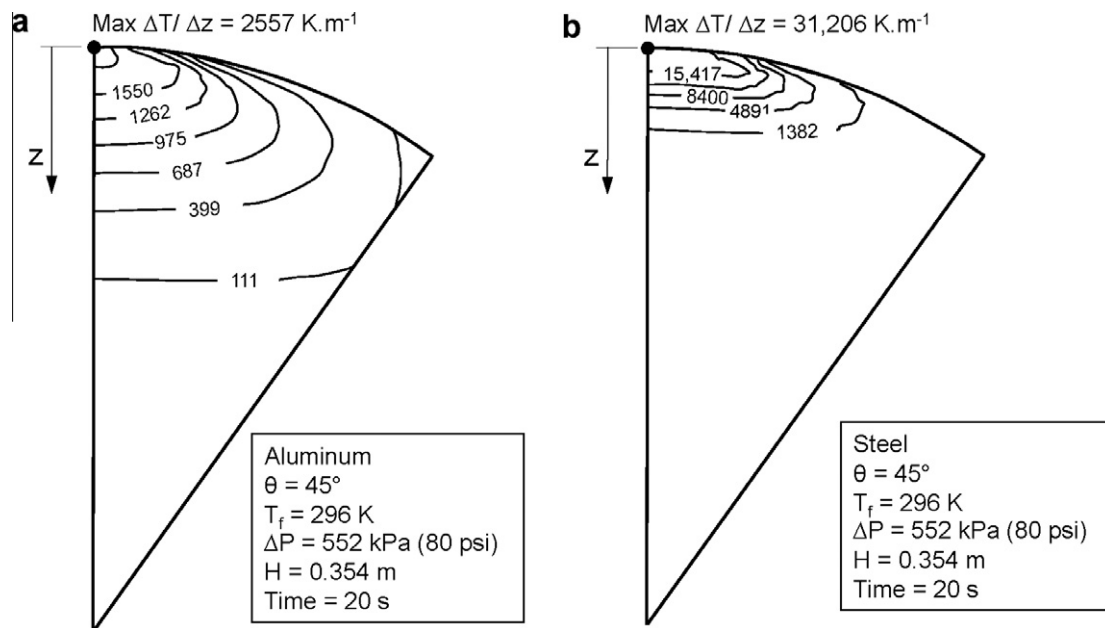


Fig. 13. Temperature gradients in unit cell 20 s into the quench for (a) aluminum and (b) steel.

with bath quenching. First, it is possible to achieve a wide range of quench rates by adjusting the nozzle height and supply pressure. By controlling those same parameters, it is possible to hasten the onset of transition boiling, which greatly enhances overall quench rate. Second, spray cooling provides high heat removal rates and therefore fast quench rates. Third, optimal configuration of a spray cooling system ensures both uniform and predictable quench behavior. Fourth, a better understanding of spray cooling behavior, with the aid of both the volumetric distribution model derived in this study and the coupling between this model and the boiling curve correlations for sprays, provides an accurate means for predicting surface temperature gradients and thermal stresses in the quenched part to guard against such part defects as stress cracks and distortions. Fifth, and most importantly, accurate spray quench curves can be combined with the alloy's temperature–time–transformation curve (also called the C-curve [25]) using the *quench-factor technique* [26] to accurately predict the hardness or strength of the metal alloy part [26–29]. A detailed discussion of how the

quench curve can be combined with the C-curve using the quench-factor technique to determine these properties is provided in [5,6].

6. Conclusions

This study examined the quenching a solid alloy cylinder using full-cone pressure sprays. A new analytical model was derived to determine the shape and size of the spray impact zone as well as the distribution of volumetric flux across the curved surface of the cylinder. This distribution was combined with heat transfer correlations for all boiling regimes and transition points associated with spray cooling to generate a local boiling curve for every location across the impact surface. Using these boiling curves as boundary conditions, a transient analysis was carried out for aluminum alloy and steel cylinders subject to different values of spray nozzle pressure drop and orifice-to-surface distance. Important findings from the study are as follows:

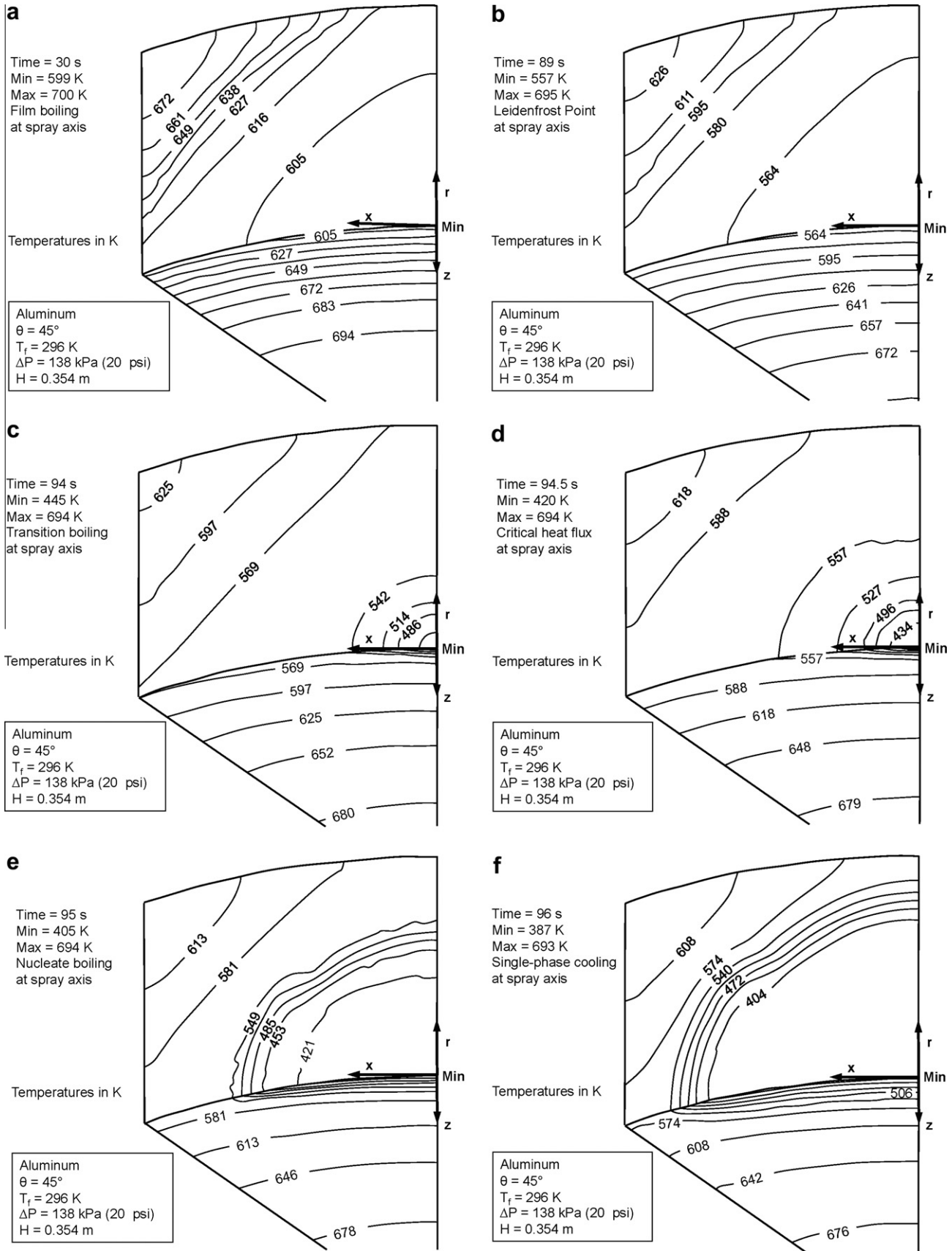


Fig. 14. Temperature contour plots in aluminum unit cell during spray quench with $\Delta P = 138 \text{ kPa (20 psi)}$ and $H = 80.354 \text{ m}$ corresponding to times when surface at spray axis is (a) in film boiling, (b) at Leidenfrost point, (c) in transition boiling, (d) at critical heat flux point, (e) in nucleate boiling, and (f) in single-phase liquid cooling regime.

1. The spray impact zone on the surface of the cylinder is elliptical in shape. The size of this zone can be increased by increasing the orifice-to-surface distance, requiring fewer nozzles to quench cylinder's circumference.
2. Volumetric flux increases with increasing nozzle pressure drop or decreasing orifice-to-surface distance. The volumetric flux is highest at the nozzle axis, and decreases towards the outer periphery of the impact zone.
3. Increasing the nozzle pressure drop or decreasing the orifice-to-surface distance causes the transitions to the lower temperature boiling regimes to occur at higher surface temperatures.
4. Points across the sprayed surface are characterized by fairly conventional spray quench curves, while points deeper within the cylinder display more gradual and slower cooling due to delays caused by heat diffusions effects.
5. Relatively high thermal diffusivity caused faster transmission of the spray cooling effect and milder temperature gradients in the aluminum alloy cylinder compared to steel. This also causes the outer surface to cool earlier but deeper points much slower for the steel cylinder.
6. Increasing the nozzle pressure drop or decreasing the orifice-to-surface distance hasten the exit from the poor film boiling regime to the more efficient transition boiling regime, resulting in a quicker quench.
7. During the quench, large thermal gradients occur momentarily on the surface because of different boiling regimes occurring at different locations exposed to the spray. The surface temperature is lowest at the spray axis, and is characterized by elliptical contours that demarcate transitions to higher temperatures towards the outer periphery of the spray zone.
8. The findings of this study highlight several practical advantages associated with the application of sprays for quenching of solid cylinders as compared with bath quenching. These include the ability to achieve a wide range of fast quench rates, uniformity and predictability of quench rate when implemented with an optimal spray configuration, ability to predict and guard against imperfections caused by thermal stresses, and the ability to predict detailed spatial distributions of mechanical properties such as hardness and strength.

Acknowledgement

The authors are grateful for the support of the Office of Naval Research (ONR) for this study.

References

- [1] S. Toda, A study in mist cooling (1st report: investigation of mist cooling), *Trans. JSME* 38 (1972) 581–588.
- [2] G.E. Totten, C.E. Bates, N.A. Clinton, *Handbook of Quenchants and Quenching Technology*, ASM International, Materials Park, OH, 1993.
- [3] L. Lin, R. Ponnappan, Heat transfer characteristics of spray cooling in a closed loop, *Int. J. Heat Mass Transfer* 46 (2003) 3737–3746.
- [4] D.P. Rini, R.-H. Chen, L.C. Chow, Bubble behavior and nucleate boiling heat transfer in saturated FC-72 spray cooling, *J. Heat Transfer* 124 (2002) 63–72.
- [5] D.D. Hall, I. Mudawar, Predicting the impact of quenching on mechanical properties of complex-shaped aluminum alloy parts, *J. Heat Transfer* 117 (1995) 479–488.
- [6] D.D. Hall, I. Mudawar, Experimental and numerical study of quenching complex-shaped metallic alloys with multiple, overlapping sprays, *Int. J. Heat Mass Transfer* 38 (1995) 1201–1216.
- [7] I. Mudawar, W.S. Valentine, Determination of the local quench curve for spray-cooled metallic surfaces, *J. Heat Treat.* 7 (1989) 107–121.
- [8] R.-H. Chen, L.C. Chow, J.E. Navedo, Effects of spray characteristics on critical heat flux in subcooled water spray cooling, *Int. J. Heat Mass Transfer* 45 (2002) 4033–4043.
- [9] I. Mudawar, K.A. Estes, Optimizing and predicting CHF in spray cooling of a square surface, *J. Heat Transfer* 118 (1996) 672–680.
- [10] J.R. Rybicki, I. Mudawar, Single-phase and two-phase cooling characteristics of upward-facing and downward-facing sprays, *Int. J. Heat Mass Transfer* 49 (2006) 5–16.
- [11] K.A. Estes, I. Mudawar, Correlation of Sauter mean diameter and critical heat flux for spray cooling of small surfaces, *Int. J. Heat Mass Transfer* 38 (1995) 2985–2996.
- [12] J.W. Hodgson, R.T. Saterbak, J.E. Sunderland, An experimental investigation of heat transfer from a spray cooled isothermal cylinder, *J. Heat Transfer* 90 (1968) 457–463.
- [13] L.D. Albright, Cooling short cylinders in air using a water spray, *Trans. Amer. Inst. Agric. Eng.* 19 (1976) 762–765.
- [14] F.P. Buckingham, A. Haji-Sheikh, Cooling of high-temperature cylindrical surfaces using a water-air spray, *J. Heat Transfer* 117 (1995) 1018–1027.
- [15] T.-B. Chang, Effects of nozzle configuration on a shell-and-tube spray evaporator with liquid catcher, *Appl. Therm. Eng.* 26 (2006) 814–823.
- [16] S.A. Moeykens, W.W. Huebsch, M.B. Pate, Heat transfer of R-134a in single-tube spray evaporation including lubrication effects and enhanced surface results, *Trans. ASHRAE* 101 (1995) 111–123.
- [17] S.A. Moeykens, M.B. Pate, The effects of nozzle height and orifice size on spray evaporation heat transfer performance for a low-finned, triangular-pitch tube bundle with R-134a, *Trans. ASHRAE* 101 (1995) 420–433.
- [18] S.A. Moeykens, J.E. Kelly, M.B. Pate, Spray evaporation heat transfer performance of R-123 in tube bundles, *Trans. ASHRAE* 102 (1996) 259–272.
- [19] I.T. Elperin, Heat transfer of two-phase flow with a bundle of tubes, *Inzhererno-FizicheskiZhurnal* 4 (1961) 30–35.
- [20] E.W. Takahara, Experimental study of heat transfer from a heated circular cylinder in two-phase, water-air flow, M.S. Thesis, Air Force Institute of Technology, Wright-Patterson AFB, OH, 1966.
- [21] D.D. Hall, A Method of Predicting and Optimizing the Thermal History and Resulting Mechanical Properties of Aluminum Alloy Parts Subjected to Spray Quenching, Purdue University, West Lafayette, IN, 1993.
- [22] H.E. Boyer, T.L. Gall (Eds.), *Metals handbook*, American Society for Metals, Materials Park, OH, 1985.
- [23] W.P. Klinzing, J.C. Rozzi, I. Mudawar, Film and transition boiling correlations for quenching of hot surfaces with water sprays, *J. Heat Treat.* 9 (1992) 91–103.
- [24] D.D. Hall, I. Mudawar, R.E. Morgan, S.L. Ehlers, Validation of a systematic approach to modeling spray quenching of aluminum alloy extrusions, composites and continuous castings, *J. Mater. Eng. Perform.* 6 (1997) 77–92.
- [25] W.L. Fink, L.A. Willey, Quenching of 75S aluminum alloy, *Trans. Amer. Inst. Min. Metall. Eng.* 175 (1948) 414–427.
- [26] J.W. Evancho, J.T. Staley, Kinetics of precipitation in aluminum alloys during continuous cooling, *Metall. Trans.* 5 (1974) 43–47.
- [27] J.T. Staley, Quench factor analysis of aluminum alloys, *Mater. Sci. Technol.* 3 (1987) 923–935.
- [28] J.W. Cahn, Transformation kinetics during continuous cooling, *Acta Metall.* 4 (1956) 572–575.
- [29] C.E. Bates, Predicting properties and minimizing residual stress in quenched steel parts, *J. Heat Treat.* 6 (1988) 27–45.